White Rose Research Online

eprints@whiterose.ac.uk
https://eprints.whiterose.ac.uk
Universities of Leeds, Sheffield and York

Deposited via The University of Leeds.

White Rose Research Online URL for this paper:
https://eprints.whiterose.ac.uk/id/eprint/109807/

Version: Accepted Version

Article:
Campbell, JM, Meldrum, FC and Christenson, HK (2017) Observing the Formation of Ice and Organic Crystals in Active Sites. Proceedings of the National Academy of Sciences, 114 (5). pp. 810-815. ISSN: 0027-8424

https://doi.org/10.1073/pnas.1617717114

© 2016, National Academy of Sciences . This is an author produced version of a paper published in Proceedings of the National Academy of Sciences. Uploaded in accordance with the publisher's self-archiving policy. In order to comply with the publisher requirements the University does not require the author to sign a non-exclusive licence for this paper.

Reuse
Items deposited in White Rose Research Online are protected by copyright, with all rights reserved unless indicated otherwise. They may be downloaded and/or printed for private study, or other acts as permitted by national copyright laws. The publisher or other rights holders may allow further reproduction and re-use of the full text version. This is indicated by the licence information on the White Rose Research Online record for the item.

Takedown
If you consider content in White Rose Research Online to be in breach of UK law, please notify us by emailing eprints@whiterose.ac.uk including the URL of the record and the reason for the withdrawal request.

UNIVERSITY OF LEEDS
University of Sheffield
UNIVERSITY of York

Observing the Formation of Ice and Organic Crystals in Active Sites

James M. Campbell[1], Fiona C. Meldrum[2] and Hugo K. Christenson[1]

[1]School of Physics and Astronomy, University of Leeds, Leeds, LS2 9JT, United Kingdom

[2]School of Chemistry, University of Leeds, Woodhouse Lane, Leeds, LS2 9JT, United Kingdom.

Corresponding author: Hugo Christenson, School of Physics and Astronomy, University of Leeds, Woodhouse Lane, Leeds, LS2 9JT, UK. 0113 343 3879, h.k.christenson@leeds.ac.uk.

PHYSICAL SCIENCES: Applied Physical Sciences

Keywords: nucleation, topography, confinement, pores, active sites

Abstract

Heterogeneous nucleation is vital to a wide range of areas as diverse as ice nucleation on atmospheric aerosols and the fabrication of high-performance thin films. There is excellent evidence that surface topography is a key factor in directing crystallisation in real systems, however the mechanisms by which nanoscale pits and pores promote nucleation remain unclear. Here, we use natural cleavage defects on Muscovite mica to investigate the activity of topographical features in the nucleation from vapour of ice and various organic crystals. Direct observation of crystallisation within surface pockets using optical microscopy, and also interferometry, both demonstrate that these sharply acute features provide extremely effective nucleation sites, and allows us to determine the mechanism by which this occurs. A confined phase is first seen to form along the apex of the wedge, and then grows out of the pocket opening to generate a bulk crystal after a threshold saturation has been achieved. Ice nucleation proceeds in a comparable manner, although our resolution is insufficient to directly observe a condensate prior to the growth of a bulk crystal. These results provide new insight into the mechanism of crystal deposition from vapour on real surfaces, where this will ultimately enable us to use topography to control crystal deposition on surfaces. They are also particularly relevant to our understanding of processes such as cirrus cloud formation, where such topographical features are likely candidates for the "active sites" that make clay particles effective nucleants for ice in the atmosphere.

Significance Statement

Crystal nucleation - the first appearance of a crystalline phase where there was none before - usually occurs at the surface of a foreign material. Ice formation in the atmosphere is dependent upon the number and type of aerosol particles present, but little is known about why some are more effective than others. Here we investigate the role of surface topography in promoting crystallisation of ice and different organic crystals and show that acute geometries are highly effective in promoting the growth of a confined crystalline phase, which then gives rise to a bulk phase. This is relevant to crystallisation in a large number of real world systems such as industrial film growth and our climate.

Introduction

The growth of a new phase is almost always dependent on a nucleation event. Nucleation is therefore fundamental to a number of processes including crystallisation, freezing, condensation and bubble formation and is typically described in terms of classical nucleation theory. However, as this theory was developed to describe the nucleation of liquid droplets in vapour, it cannot give a complete understanding of all nucleation processes, and in particular the formation of crystalline materials. Nucleation in the real world is also usually heterogeneous, occurring on seeds, impurities, or container surfaces. Although simple models consider nucleation to occur on perfectly flat, uniform surfaces, it is clear that real surfaces inevitably vary in chemistry and topography. We focus here on the effects of surface topography. Classical nucleation theory predicts a lower free energy barrier to nucleation in surface cracks or pores on the length scale of a critical nucleus.(1) The extent of the reduction is contact-angle dependent, such that nuclei with a low contact angle experience a more significant reduction from topography.

Topography is known to promote crystallisation directly from a vapour (2-5), as these systems typically exhibit low contact angles. Crystallisation from the melt, in contrast, is associated with very high contact angles such that topography is usually ineffective (6). Crystallisation from solution provides an intermediate case, and has perhaps received the most attention. Roughened surfaces have been shown to enhance the nucleation of a range of crystals (7-10), while the nucleation of proteins and organic crystals is promoted within narrow pores of specific diameters.(11-13) The geometries of these pores can even determine the orientation and polymorphs of the product crystals.(14-16) However, while these data provide strong evidence for the importance of surface topography to nucleation, we still have little knowledge of what makes a good nucleation site, or how such sites function on the nanoscale.

One area where these questions have been considered is atmospheric ice nucleation. It has been suggested that surfaces could exhibit a small number of "active sites" which determine the nucleating ability of an entire surface.(17-19) Each site has its own threshold supersaturation or supercooling above which nucleation becomes probable,(20, 21) and the sites with the lowest thresholds dominate. Fukuta then suggested that ice nucleation from vapour may proceed by the formation of confined condensates within small pores and cracks, and that bulk crystals emerge from these upon sufficient saturation of water vapour.(22) To understand heterogeneous nucleation, we therefore need to understand how these active sites promote it.

The current study addresses this challenge by investigating the nucleation from vapour of ice and a number of organic compounds within a well-defined topographical feature – the "pockets" that are commonly formed along the steps on cleaved mica substrates. Featuring a highly acute wedge geometry, these structures are possible candidates for the active sites present on clay/dust particles that drive atmospheric ice nucleation. Importantly, we can use optical microscopy to both characterise the geometry of these pockets and to monitor crystallisation *in situ* within them. Our results show that the mica pockets are extremely effective nucleation sites for every compound we have exposed them to. We also provide direct experimental evidence for a condensate-mediated method of nucleation, where growth originates as a confined condensate along the apex of an acute wedge, with a threshold supersaturation required for growth into a bulk crystal.

Results

Substrates were prepared by cleaving Muscovite mica, which generates a pristine surface that is atomically flat over large areas (23). These surfaces often feature a number of step edges, which can themselves support a range of defects. The current study exploits one key type of defect, namely the "pockets" that are created when the top layers of mica are locally detached from those below, leaving a space in-between (Figure 1). A highly acute wedge geometry is formed where the two mica surfaces meet that would be impossible to generate using surface engineering techniques. Importantly, these pockets can be readily studied using optical interference, where the pattern of interference fringes provides information about the separation of the mica sheets at different positions within the pockets (Figure 1). Interference between reflections from the mica surfaces forming the top and bottom of the wedge produces a reflected light intensity I that is dependent on the mica-mica spacing z as described by the relation

$$I \approx I_0 + a\sin^2\frac{2\pi z}{\lambda} \quad (1)$$

where λ is the wavelength, I_0 is a background intensity from other surfaces and a a constant dependent on the reflectance (more details and exact form in Supplementary Information). As a consequence there is a bright fringe at $\lambda/4$ separation and then at intervals of $\lambda/2$. This allows a wedge profile to be precisely calculated. The pattern of these fringes also changes on deposition of liquid or solid within the pocket, such that we can monitor the entire growth sequence of crystals within these features. The presence of a condensed phase greatly reduces the reflectance of both surfaces, making I drop almost to I_0. With the additional ease of diffusion of material into these features, they are ideal for studying topographically aided nucleation.

Three organic compounds – norbornane, carbon tetrabromide and camphor – were selected for study as they have high vapour pressures and melting points well above room temperature (23-25 °C), with their physical properties presented in Supplementary Table S1. Preliminary experiments were also conducted with hexachloroethane, hexamethylcyclotrisiloxane and tetramethylbutane. These experiments were performed in a sealed cell that contains a reservoir of crystal at the base and the mica substrate at the top, where the mica can be observed throughout the experiment using an optical microscope in reflected light mode.(19) Saturation is controlled by adjusting the temperature of the reservoir with respect to that of the substrate, which is held at room temperature. The reservoir is initially cooled to 1 °C below the substrate to produce undersaturated conditions. This protocol generated highly reproducible results, as shown by the consistency of the measured saturation at the

moment of first emergence of a bulk crystal from the pocket (see Methods in the Supplementary Information).

The mica pockets provide extremely effective nucleation sites for every organic compound we studied. A distinctive pattern of growth was observed, in which twin crystals grow from the two "corners" of the pocket where the wedge apex meets the step edge (Figure 2). Crystal growth is also seen all along the apex of the wedge in each case, although this is sometimes difficult to see in low-magnification images. Figures 3a-d show high-magnification images of a norbornane condensate near to a corner (camphor and carbon tetrabromide results are qualitatively similar). A condensate begins to form in the wedge apex and then grows steadily, tending to grow thicker close to the corner, consistent with a lower diffusion barrier to growth near the corner.(24) For every organic compound, a condensate is clearly visible before a bulk crystal emerges from the pocket corner.

Ice nucleation was studied at temperatures down to -45.0 °C in a different cell (Materials and Methods, Supplementary Information), and experiments were performed by reducing the substrate temperature at 0.25 °C min^{-1} while exposed to gas flow with a steady and adjustable humidity. At nucleation temperatures of -37.0 °C and above the pocket appears to be unimportant, with liquid drops condensing on the mica surface, some of which then freeze and hence cause the others to evaporate. At -38.8 °C and below, the same mode of growth was seen as with the organics, with hexagonal or columnar ice crystals emerging from the pocket corners (Figure 2). But unlike the organics, no condensate was ever observed before the appearance of a bulk crystal, down to the observation limit of 15 nm. Figures 3e,f show the growth of ice crystals along a wedge apex at -39.0 °C, but this growth was not seen until just after the first bulk crystal growth was observed at the corner. Saturation could not be so precisely quantified as with organics, but ice was seen emerging from the pockets at a saturation of 1.2 ± 0.1 for all experiments.

The “heights” of organic condensates were quantified by taking an intensity profile across an interference fringe and finding the location of a sharp step in intensity from the condensate edge, as illustrated in Figures 1f-1h. This method is accurate to within 1 nm for condensates as small as 15 nm; smaller condensates cannot usually be unambiguously detected. The heights of condensates formed prior to the emergence of a bulk crystal are plotted in Figures 4 and 5. Norbornane condensates form in the wedge even in undersaturated conditions (Figure 5), while no evidence for the existence of condensates prior to saturation was obtained for camphor and carbon tetrabromide (Figure 4).

However, as these compounds have much lower vapour pressures than norbornane, their condensates would take longer to grow to an observable size.

This possibility was investigated further by performing experiments in which the saturations of carbon tetrabromide and camphor were allowed to approach (but never quite reach) unity slowly over several hours. The carbon tetrabromide condensate grew to 84 ± 1 nm after three hours, while that of camphor grew to 60 ± 1 nm after five hours. The influence of the temperature ramp rate on the condensation of norbornane within a single pocket was also studied (Figure 5) and showed two clear trends as the ramp rate increases: a higher saturation is required before bulk crystals emerge; and the precursor condensates are smaller in size.

Further information about the mechanism of crystallisation was obtained by performing multiple crystallisation cycles using the same mica pockets, where the cell was flushed after each run to sublime the previous crystals (in the case of ice the substrate was warmed to above 0 °C between runs). For both the organics and ice, the two bulk crystals that form at each side of a pocket were seldom in the same crystallographic orientation, as judged by their external geometries. This demonstrates that the two external crystals and connecting condensate are rarely a single crystal. There was also no evidence of a consistent orientation between runs, suggesting that the geometry of the wedge does not determine crystal orientation.

Discussion

Our results provide a striking demonstration that surface topography – and in particular features containing narrow wedges – can provide extremely effective nucleation sites, where the organic compounds studied initially deposit in the apex of the mica wedge, before growing out of the pockets as bulk crystals. The deposition of a condensed phase, be it liquid or solid, within the pockets is driven by the lower interfacial free energy between the mica substrate and the condensate compared to the interfacial free energy between the mica and the vapour. As a consequence the condensate has a contact angle below 90° and may form a concave interface, as shown in Figure 1f. The Kelvin equation describes a reduction of vapour pressure p' over a curved interface:

$$\ln \frac{p'}{p_0} = \frac{\cos\theta \cdot \gamma V_{\mathrm{m}}}{rRT} \qquad (2)$$

where p_0 is the vapour pressure over a flat surface, θ is the contact angle of the substance in the condensate on mica, γ is the compound-vapour surface free energy, V_{m} is the molar volume, r is the radius of curvature of the interface condensate, R is the gas constant and T is the temperature. For a condensate interface that is concave towards the vapour r is negative, and therefore the vapour pressure is reduced below that for a flat surface. Thus, any substance can condense in an acute wedge slightly below saturation, provided that θ is below 90°, which is known as capillary condensation. The largest condensates will occur when θ approaches 0°, which in our case means that $2|r| = h$, the condensate height.

We expect the first condensate formed to be a supercooled liquid, which will then freeze to form a solid condensate by normal nucleation. The Gibbs-Thomson effect predicts that a confined phase will suffer a decrease in the melting point inversely proportional to the dimension of the pore; as such, an infinitesimally small condensate is expected to be a liquid.(25) This mechanism has been experimentally observed in a highly acute annular wedge.(24-26)

Theoretically, the size of a supercooled liquid condensate is described by the Clausius-Clapeyron relation, which shows that the vapour pressure p_l over a supercooled liquid is higher than p_s over a solid at the same temperature:

$$\ln \frac{p_l}{p_s} = \frac{\Delta H_{\mathrm{fus}}}{R}\left(\frac{1}{T} - \frac{1}{T_{\mathrm{m}}}\right) \qquad (3)$$

where ΔH_{fus} is the enthalpy of fusion and T_{m} the melting point. This predicts a ratio p_l / p_s of 1.5 for water/ice at -40 °C, of 1.3 for both norbornane and carbon tetrabromide and of 2.5 for camphor at 27 °C. We therefore expect a liquid condensate to reach equilibrium at a smaller size than a solid one in

the same conditions. The height h of a liquid condensate, assuming $\theta = 0$, at solid saturation may be estimated by combining equations 2 and 3:

$$\frac{\gamma V_{\mathrm{m}}}{rT} = \frac{2\gamma V_{\mathrm{m}}}{hT} \approx \Delta H_{\mathrm{fus}}\left(\frac{1}{T} - \frac{1}{T_{\mathrm{m}}}\right) \tag{4}$$

where γ here refers to liquid-vapour surface tension. At $T \ll T_m$ this is only approximate (25). Values of h are predicted in Table 1.

Following this argument, are the condensates that we here observe supercooled liquids or solids? Figure 5 shows the estimated equilibrium heights of solid and liquid norbornane condensates, assuming θ = 0°. These lines give the maximum sizes these condensates could reach if they were left sufficiently long to equilibrate at any given saturation. The observed condensate heights are well above those possible for a liquid condensate, which provides conclusive evidence that the measured condensates are solid. As Table 1 shows, the expected height of the liquid condensates at saturation with respect to solid are below or close to the lower limit of observation for all compounds. However, this does not rule out the initial presence of a supercooled liquid condensate which then freezes to give rise to a solid condensate before the condensate grows to an observable size. Estimation of the critical nucleus radius for all of our systems (Table 1) shows that the condensate heights are more than twice the critical radii; liquid condensates of this size are large enough to contain a critical nucleus and are therefore metastable with respect to freezing.

So far we have discussed only the formation of a condensate inside a wedge without considering the transition into a bulk phase. As seen in Figures 3a-d, the confined condensate extends right to the pocket corner where it meets the bulk vapour. There seems to be nothing stopping the crystal from growing out into the bulk, and yet no emergence is observed until a threshold supersaturation is attained. This problem is illustrated in Figure 6, in which the condensate has a concave interface, provided that θ is below 90°. However, as it begins to bulge out of the narrow opening, it first flattens out and its curvature then becomes convex with respect to the vapour and passes through a minimum in radius of curvature. After this point it can grow unrestricted into the bulk phase. In equation 2, r changes sign, necessitating a supersaturated vapour. The minimum in the convex radius of curvature defines a minimum or threshold supersaturation necessary for the condensate to emerge from the pore. Taking this minimum radius to be equal to the pore radius, the threshold saturation S is given by the Kelvin equation:

$$\ln S = \frac{\gamma V_m}{rRT} \quad (5)$$

It follows that the narrower the mica-mica separation at the pore opening, the higher the saturation needed for a bulk phase to emerge. This concept has been verified in simulations by Page and Sear,(27) who show that there is a free energy barrier for a crystal to emerge from a narrow pore, which does not exist if the saturation is sufficiently high.

While this is clearly a simplified model of our system, it works well to illustrate general trends. The edge of our system can be seen as a slit pore which increases in width with increasing distance from the wedge apex. When a condensate is very small, the mica-mica spacing is too narrow for it to emerge at modest supersaturation (the energy barrier is too large). As the supersaturation increases, the condensate grows further from the apex such that the width of the gap from which the condensate must emerge also increases. At some point the saturation exceeds the threshold for growth through the gap, and a bulk crystal emerges. The threshold lines for camphor and carbon tetrabromide, and for norbornane are shown in Figures 4 and 5, respectively. While our data are in good agreement with these at low rates of saturation increase, at the higher rates used with norbornane the condensate size and saturation increase significantly beyond the point where emergence would be expected. However, at high rates of crystal growth it is likely that the local supersaturation is no longer accurately given by the temperature difference between substrate and reservoir.

In the case of ice, no condensates were seen prior to the growth of bulk crystals. Rather than implying that there were no condensates, it is extremely likely that the condensates were simply too small to observe (below 15 nm) up to the moment of bulk emergence. The nature of growth, with two crystals at the pocket corners and a continuous line of crystal growth along the wedge apex, is strikingly reminiscent of results with organic compounds where condensates were observed prior to growth (Figure 2). Ice at -40 °C has a significantly lower vapour pressure than any of the other compounds studied, and the ramp rate into supersaturated conditions was faster, so observably large ice condensates may not have had sufficient time to form. Equation 5 predicts that a 15 nm ice condensate could emerge into a bulk phase at a modest saturation of 1.13, so if this saturation was attained before the condensates grew to visible size, we would not expect further growth before the appearance of a bulk crystal. It is also possible that the condensate was supercooled water, which on freezing would begin to grow all along the wedge apex at the same time as the bulk crystal emerges, as was observed. As seen in Table 1, the water condensate would be below the 15 nm limit of observation. Calculating the volume of water in a condensate at ice saturation in a 1 mm-long wedge

with a constant 0.3° angle and extrapolating published ice nucleation rates (28), we estimate that we would expect to see one nucleation event every 1.2 minutes at -39 °C. On the time-scale of these experiments (a ramp rate of 0.25 °C/min) it is plausible that ice nucleation from water is the limiting step in the process.

The results with ice are immediately relevant to atmospheric ice nucleation on solid aerosol particles. Most studies of atmospheric ice nucleation have focused on the importance of surface chemistry and lattice matching. However, the correlation between lattice match and nucleation is in general not strong,(29) and there is a wide scatter in the reported nucleating abilities of atmospheric aerosols (30). The mechanism of ice nucleation in capillary-condensed water that was proposed fifty years ago by Fukuta has only recently been re-visited (31, 32), but it has already been suggested that it contributes to the ice nucleation capacity of kaolinite (33, 34), and leads to enhanced ice nucleation by porous aerosol particles (35, 36). It is also noteworthy that alkali feldspars, which have been shown to be particularly efficient ice nucleators (37) usually have a rich microstructure (38) with an abundance of sites where water might condense. We have now directly observed how nucleation via condensed, supercooled water is an important mechanism for nucleation of ice in cleavage defects on mica, thereby highlighting the importance of pore condensation freezing in atmospheric ice nucleation.

Conclusions

These results provide direct experimental evidence that highly acute wedges – the key feature of the mica pockets studied here – are extremely effective nucleation sites for crystallisation from vapour. Using direct imaging approaches we demonstrate that bulk crystals form subsequent to generation of a confined condensate in the acute wedge, where this can even occur in undersaturated conditions. Although we employed micron-scale topographical features for the purpose of easy and unambiguous condensate observation, the principles should equally apply to smaller features that may occur on natural or engineered surfaces. The only compulsory feature is that they must possess a geometry acute enough to allow condensation without an energy barrier. This model also suggests that there will be an optimal feature size for any given supersaturation. Features which are too small may fill quickly but have too narrow an opening to allow emergence into a bulk phase. Conversely, large features may take so long to fill that crystals may have already emerged from smaller features. This phenomenon clearly has many real-world applications. Crystal nucleation from vapour is a vital process in atmospheric science and in technological applications such as Chemical Vapour Deposition film growth. An analogous thermodynamic pathway to nucleation has even been proposed to occur in solution during the formation of biominerals such as calcium carbonate from amorphous precursor phases.(39) Understanding topographically-directed crystallisation, and identification of the most active features, therefore promises a novel strategy for controlling nucleation in a wide range of environments.

Acknowledgements

HKC acknowledges a grant from the Leverhulme Trust (RPG-2014-306), and HKC and FCM acknowledge support from the EPSRC (EP/M003027/1 and EP/N002423/1).

References

1. Sholl CA & Fletcher NH (1970) Decoration criteria for surface steps. *Acta Metall* 18(10):1083-1086.
2. Buijnsters JG, Vázquez L, & Ter Meulen JJ (2009) Substrate pre-treatment by ultrasonication with diamond powder mixtures for nucleation enhancement in diamond film growth. *Diam Relat Mater* 18(10):1239-1246.
3. Dennig PA & Stevenson DA (1991) Influence of substrate topography on the nucleation of diamond thin films. *Appl Phys Lett* 59(13):1562-1564.
4. Portavoce A, Kammler M, Hull R, Reuter MC, & Ross FM (2006) Mechanism of the nanoscale localization of Ge quantum dot nucleation on focused ion beam templated Si(001) surfaces. *Nanotechnology* 17(17):4451.
5. Holbrough JL, Campbell JM, Meldrum FC, & Christenson HK (2012) Topographical control of crystal nucleation. *Cryst Growth Des* 12(2):750-755.
6. Campbell JM, Meldrum FC, & Christenson HK (2015) Is ice nucleation from supercooled water insensitive to surface roughness? *J Phys Chem C* 119(2):1164-1169.
7. Diao Y, Myerson AS, Hatton TA, & Trout BL (2011) Surface design for controlled crystallization: The role of surface chemistry and nanoscale pores in heterogeneous nucleation. *Langmuir* 27(9):5324-5334.
8. Sengupta Ghatak A & Ghatak A (2013) Disordered nanowrinkle substrates for inducing crystallization over a wide range of concentration of protein and precipitant. *Langmuir* 29(13):4373-4380.
9. Järn M, Areva S, Pore V, Peltonen J, & Linden M (2006) Topography and surface energy dependent calcium phosphate formation on sol-gel derived TiO_2 coatings. *Langmuir* 22(19):8209-8213.
10. Asanithi P (2014) Surface porosity and roughness of micrographite film for nucleation of hydroxyapatite. *J Biomed Mater Res-A* 102(8):2590-2599.
11. Ha J-M, Wolf JH, Hillmyer MA, & Ward MD (2004) Polymorph selectivity under nanoscopic confinement. *J Am Chem Soc* 126(11):3382-3383.
12. Chayen NE, Saridakis E, & Sear RP (2006) Experiment and theory for heterogeneous nucleation of protein crystals in a porous medium. *P Natl Acad Sci USA* 103(3):597-601.
13. Shah UV, Williams DR, & Heng JYY (2012) Selective crystallization of proteins using engineered nanonucleants. *Cryst Growth Des* 12(3):1362-1369.
14. Diao Y, Harada T, Myerson AS, Hatton TA, & Trout BL (2011) The role of nanopore shape in surface-induced crystallization. *Nat Mater* 10(11):867-871.
15. Mitchell CA, Yu L, & Ward MD (2001) Selective nucleation and discovery of organic polymorphs through epitaxy with single crystal substrates. *J Am Chem Soc* 123(44):10830-10839.
16. Cantaert B, Beniash E, & Meldrum FC (2013) Nanoscale confinement controls the crystallization of calcium phosphate: relevance to bone formation. *Chem-Eur J* 19(44):14918-14924.

17. Fletcher NH (1969) Active sites and ice crystal nucleation. *J Atmos Sci* 26(6):1266-1271.

18. Niedermeier D*, et al.* (2011) Heterogeneous ice nucleation: exploring the transition from stochastic to singular freezing behavior. *Atmos Chem Phys* 11(16):8767-8775.

19. Campbell JM, Meldrum FC, & Christenson HK (2013) Characterization of preferred crystal nucleation sites on mica surfaces. *Cryst Growth Des* 13(5):1915-1925.

20. Dorsey NE (1938) Supercooling and freezing of water. *J Res Natl Bureau Standards* 20(6):799-808.

21. Vali G (2014) Interpretation of freezing nucleation experiments: singular and stochastic; sites and surfaces. *Atmos Chem Phys* 14(11):5271-5294.

22. Fukuta N (1966) Activation of atmospheric particles as ice nuclei in cold and dry air. *J Atmos Sci* 23(6):741-750.

23. Christenson HK & Thomson NH (2016) The nature of the air-cleaved mica surface. *Surf Sci Rep* 71(2):367-390.

24. Kovács T & Christenson HK (2012) A two-step mechanism for crystal nucleation without supersaturation. *Faraday Discuss* 159(1):123-138.

25. Nowak D, Heuberger M, Zäch M, & Christenson HK (2008) Thermodynamic and kinetic supercooling of liquid in a wedge pore. *J Chem Phys* 129(15):154509.

26. Kovács T, Meldrum FC, & Christenson HK (2012) Crystal nucleation without supersaturation. *J Phys Chem Lett* 3(12):1602-1606.

27. Page AJ & Sear RP (2006) Heterogeneous nucleation in and out of pores. *Phys Rev Lett* 97(6):065701.

28. Murray BJ*, et al.* (2010) Kinetics of the homogeneous freezing of water. *Phys Chem Chem Phys* 12(35):10380-10387.

29. Conrad P, Ewing GE, Karlinsey RL, & Sadtchenko V (2005) Ice nucleation on BaF_2 (111). *J Chem Phys* 122(6):064709-064709.

30. Hoose C & Möhler O (2012) Heterogeneous ice nucleation on atmospheric aerosols: a review of results from laboratory experiments. *Atmos Chem Phys* 12(20):9817-9854.

31. Christenson HK (2013) Two-step crystal nucleation via capillary condensation. *Cryst Eng Comm* 15(11):2030-2039.

32. Marcolli C (2014) Deposition nucleation viewed as homogeneous or immersion freezing in pores and cavities. *Atmos Chem Phys* 14(4):2071-2104.

33. Welti A, Kanji ZA, Lüönd F, Stetzer O, & Lohmann U (2014) Exploring the mechanisms of ice nucleation on kaolinite: from deposition nucleation to condensation freezing. *J Atmos Sci* 71(1):16-36.

34. Wang B*, et al.* (2016) Direct observation of ice nucleation events on individual atmospheric particles. *Phys Chem Chem Phys* 18(43):29721-29731.

35. Adler G*, et al.* (2013) Formation of highly porous aerosol particles by atmospheric freeze-drying in ice clouds. *P Natl Acad Sci USA* 110(51):20414-20419.

36. Wagner R, Kiselev A, Möhler O, Saathoff H, & Steinke I (2016) Pre-activation of ice-nucleating particles by the pore condensation and freezing mechanism. *Atmos Chem Phys* 16(4):2025-2042.

37. Yakobi-Hancock JD, Ladino LA, & Abbatt JPD (2013) Feldspar minerals as efficient deposition ice nuclei. *Atmos Chem Phys* 13(22):11175-11185.

38. Parsons I, Lee MR, & Smith JV (1998) Biochemical evolution II: Origin of life in tubular microstructures on weathered feldspar surfaces. *P Natl Acad Sci USA* 95(26):15173-15176.

39. Stephens CJ, Ladden SF, Meldrum FC, & Christenson HK (2010) Amorphous calcium carbonate is stabilized in confinement. *Adv Funct Mater* 20(13):2108-2115.

40. Bailey AI & Kay SM (1965) Measurement of refractive index and dispersion of mica, employing multiple beam interference techniques. *Brit J Appl Phys* 16(1):39.

41. Hacker PT (1951) *Experimental values of the surface tension of supercooled water* (National Advisory Committee for Aeronautics).

42. Hillig WB (1998) Measurement of interfacial free energy for ice/water system. *J Cryst Growth* 183(3):463-468.

43. Böyük U & Maraşlı N (2009) Interfacial energies of carbon tetrabromide. *Curr Appl Phys* 9(2):359-366.

44. Haynes WM (2016) *CRC handbook of chemistry and physics* (CRC press).

45. Boublík T, Fried V, & Hála E (1984) *The vapour pressures of pure substances* (Elsevier).

46. Bradley RS & Drury T (1959) The vapour pressure and lattice energy of carbon tetrabromide. *T Faraday Soc* 55:1844-1847.

47. Murphy DM & Koop T (2005) Review of the vapour pressures of ice and supercooled water for atmospheric applications. *Q J Roy Meteor Soc* 131(608):1539-1565.

48. Boyd RH, Sanwal SN, Shary-Tehrany S, & McNally D (1971) Thermochemistry, thermodynamic functions, and molecular structures of some cyclic hydrocarbons. *J Phys Chem* 75(9):1264-1271.

49. Rietveld IB*, et al.* (2010) Temperature and composition-dependent properties of the two-component system d-and l-camphor at 'ordinary'pressure. *Thermochim Acta* 511(1):43-50.

50. Yaws CL & Gabbula C (2003) *Yaws' Handbook of Thermodynamic and Physical Properties of Chemical Compounds* (Knovel).

51. Feistel R & Wagner W (2007) Sublimation pressure and sublimation enthalpy of H_2O ice I_h between 0 and 273.16 K. *Geochim Cosmochim Ac* 71(1):36-45.

52. ChemSpider (Accessed 2016-10-11) www.chemspider.com. (Royal Society of Chemistry).

53. Weast RC (1987) *CRC Handbook of Chemistry and Physics* (CRC Press).

54. Ketcham WM & Hobbs PV (1969) An experimental determination of the surface energies of ice. *Philos Mag* 19(162):1161-1173.

Table 1. Classical nucleation theory predictions for size of critical nucleus radius (r*) and free energy barrier ($\Delta\mu$*). h is the predicted size of a liquid condensate at saturation with respect to a solid.

Compound	r* (nm)	h (nm)	$\Delta\mu$* (kT)
norbornane (27 °C)	2.8	9.1	82
carbon tetrabromide (27 °C)	2.3	16	35
camphor (27 °C)	1.3	4.3	18
ice (-39 °C)	1.5	3.9	92

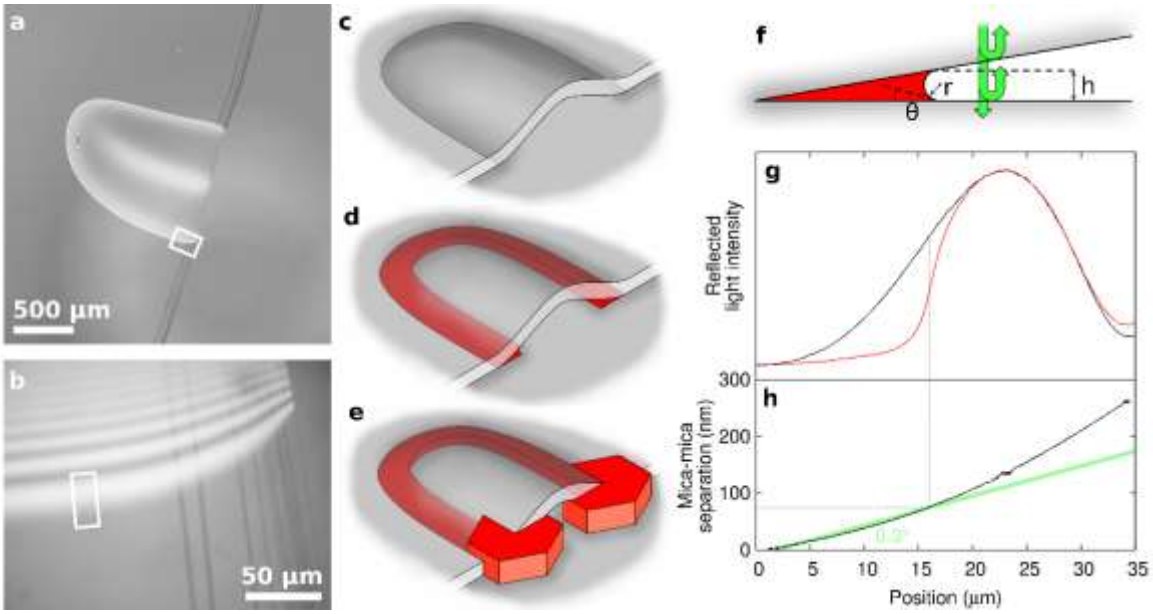

Figure 1. Experimental overview. (a) Optical micrograph of a pocket, and (b) a higher-magnification view of the region outlined in white, showing interference fringes. (c) Schematic illustration of a pocket, and (d) and (e) the growth of a crystalline condensate (in red) which then leads to the growth of twin bulk crystals. (f) A condensate forming in an acute wedge, where the twin reflections of light from closely-spaced mica surfaces (green arrows) leads to interference fringes; also showing condensate height h, interface radius of curvature r and contact angle θ. (g) Light intensity curves across a single fringe highlighted in white in (b), corresponding to an empty wedge (black) and a wedge holding a 75 nm condensate of carbon tetrabromide (red). The condensate is visible as a relatively sharp cut-off of fringe intensity. (h) The wedge profile calculated from the black curve in (g), with a 0.3° angle shown in green for reference.

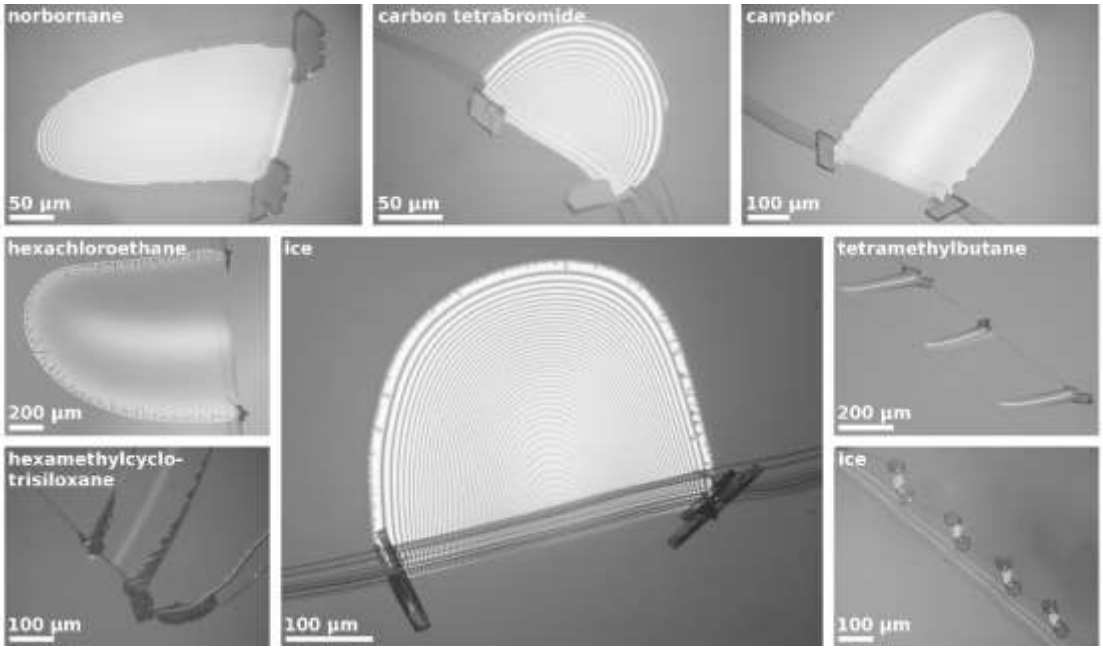

Figure 2. Optical micrographs showing crystals of various compounds crystallising from the two corners of one or more mica pockets.

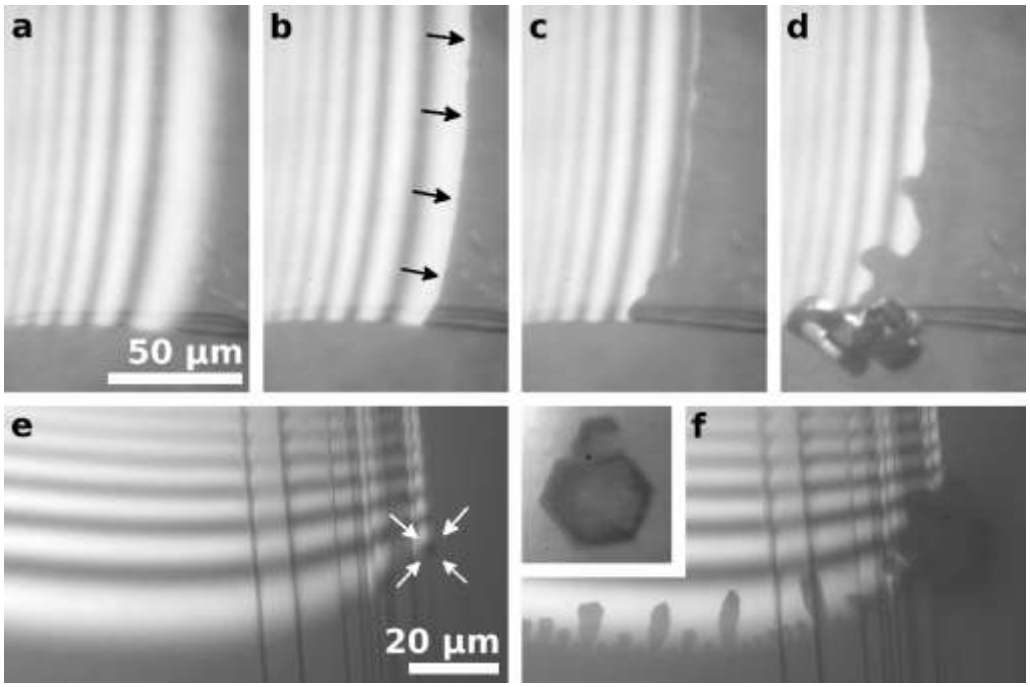

Figure 3. Optical micrographs showing crystal nucleation of norbornane (a-d, pocket opening at bottom of images) and ice (e-f, pocket opening at right of images) in the corners of mica pockets. Where a condensate exists it is visible as a sharp step in reflected light intensity, in contrast to the gradual transition associated with an empty wedge. Norbornane: (a) empty wedge, (b) small condensate below $\lambda/4$ high (indicated by black arrows), (c) larger condensate just before emergence of a bulk crystal, and (d) after emergence of a bulk crystal. Ice (at -39.0 °C): (e) the white arrows indicate the first appearance of an ice crystal at the pocket corner, with no condensate yet visible along the wedge apex; (f) subsequent growth of ice along the wedge apex. The inset shows a refocused, higher magnification view of the bulk ice crystal, demonstrating a hexagonal profile.

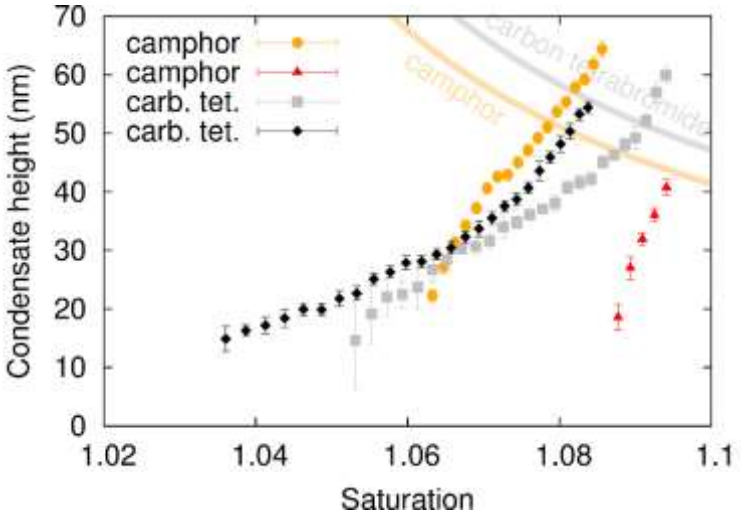

Figure 4. Graphs of condensate size with increasing saturation (with respect to bulk solid) for camphor and carbon tetrabromide at a ramp rate of 0.1 °C min^{-1}. The first point in each series marks the first unambiguously detectable condensate, while the last marks the first appearance of a bulk crystal emerging from the pocket corner. Error bars represent standard error in measurement of condensate heights; horizontal error bars are omitted for clarity. The grey and orange lines predict the condensate size above which there should be no barrier to emergence into a bulk crystal for carbon tetrabromide and camphor, respectively.

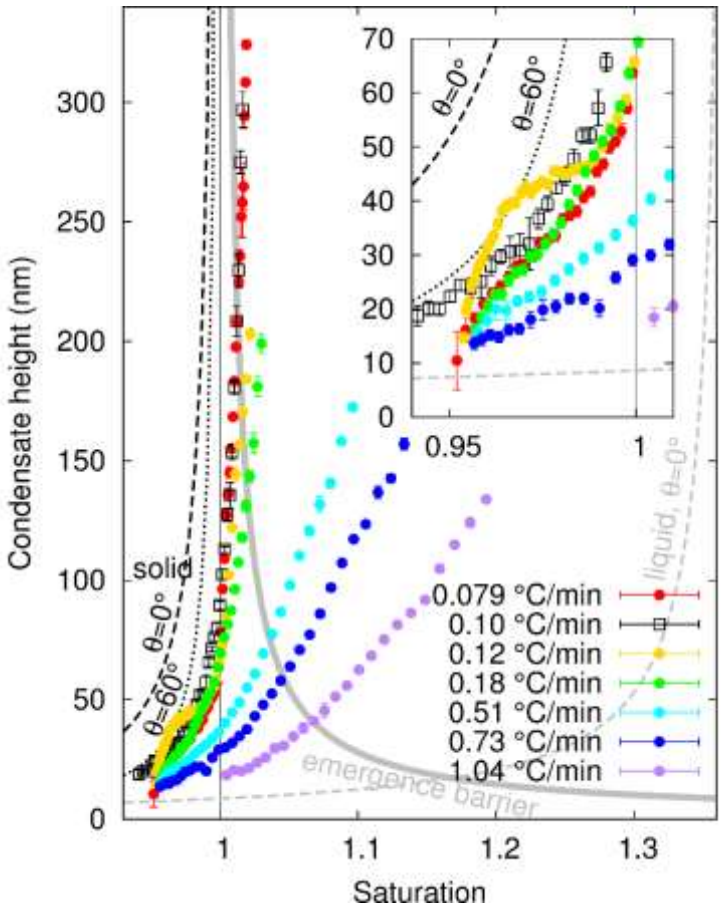

Figure 5. Graphs of norbornane condensate size with increasing saturation (with respect to bulk solid). The first point in each series marks the first unambiguously detectable condensate; the last marks the first appearance of a bulk crystal emerging from the pocket corner. The circles show growth at various temperature ramp rates in the same mica pocket, while open black squares show growth in a different pocket at 0.1 °C min^{-1}. The inset is an enlargement of the bottom-left region of the main graph. Error bars (often too small to be visible) represent standard error in measurement of condensate heights; horizontal error bars are omitted for clarity. The dashed lines show the predicted equilibrium condensate size for a solid and a liquid (black and grey respectively). The thick grey line predicts the condensate size above which there should be no barrier to emergence into a bulk crystal.

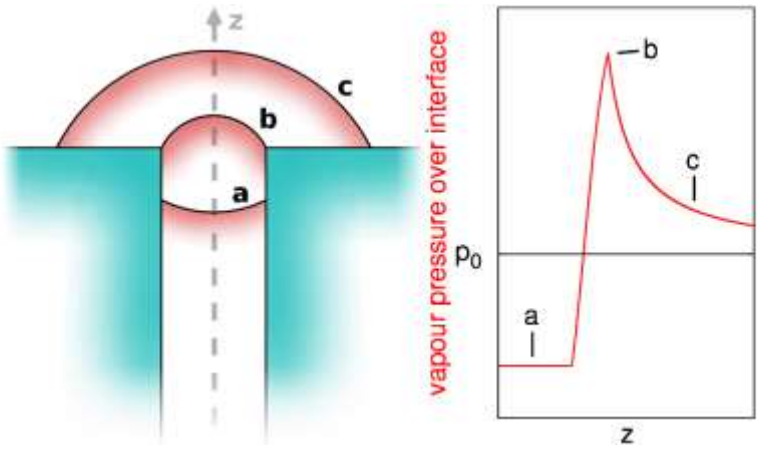

Figure 6. (left) Illustration of how a phase confined in a pore emerges into a bulk phase. (a) The phase initially has a concave interface, allowing it to be stable in confinement even in undersaturated conditions. (b) Before it can emerge into a bulk phase it must briefly form a highly convex interface, requiring supersaturation. (c) As the bulk phase grows its interface curvature reduces, tending towards a planar interface. (right) Schematic graph of the evolution of vapour pressure over the interface as the new phase emerges, with the labels a, b and c corresponding to the three stages illustrated on the left.